Cell Reports Medicine, Volume *4*

Supplemental information

Fusion-negative rhabdomyosarcoma 3D organoids to predict effective drug combinations: A proof-of-concept on cell death inducers

Clara Savary, Léa Luciana, Paul Huchedé, Arthur Tourbez, Claire Coquet, Maëlle Broustal, Alejandro Lopez Gonzalez, Clémence Deligne, Thomas Diot, Olivier Naret, Mariana Costa, Nina Meynard, Virginie Barbet, Kevin Müller, Laurie Tonon, Nicolas Gadot, Cyril Degletagne, Valéry Attignon, Sophie Léon, Christophe Vanbelle, Alexandra Bomane, Isabelle Rochet, Virginie Mournetas, Luciana Oliveira, Paul Rinaudo, Christophe Bergeron, Aurélie Dutour, Martine Cordier-Bussat, Aline Roch, Nathalie Brandenberg, Sophie El Zein, Sarah Watson, Daniel Orbach, Olivier Delattre, Frédérique Dijoud, Nadège Corradini, Cécile Picard, Delphine Maucort-Boulch, Marion Le Grand, Eddy Pasquier, Jean-Yves Blay, Marie Castets, and Laura Broutier

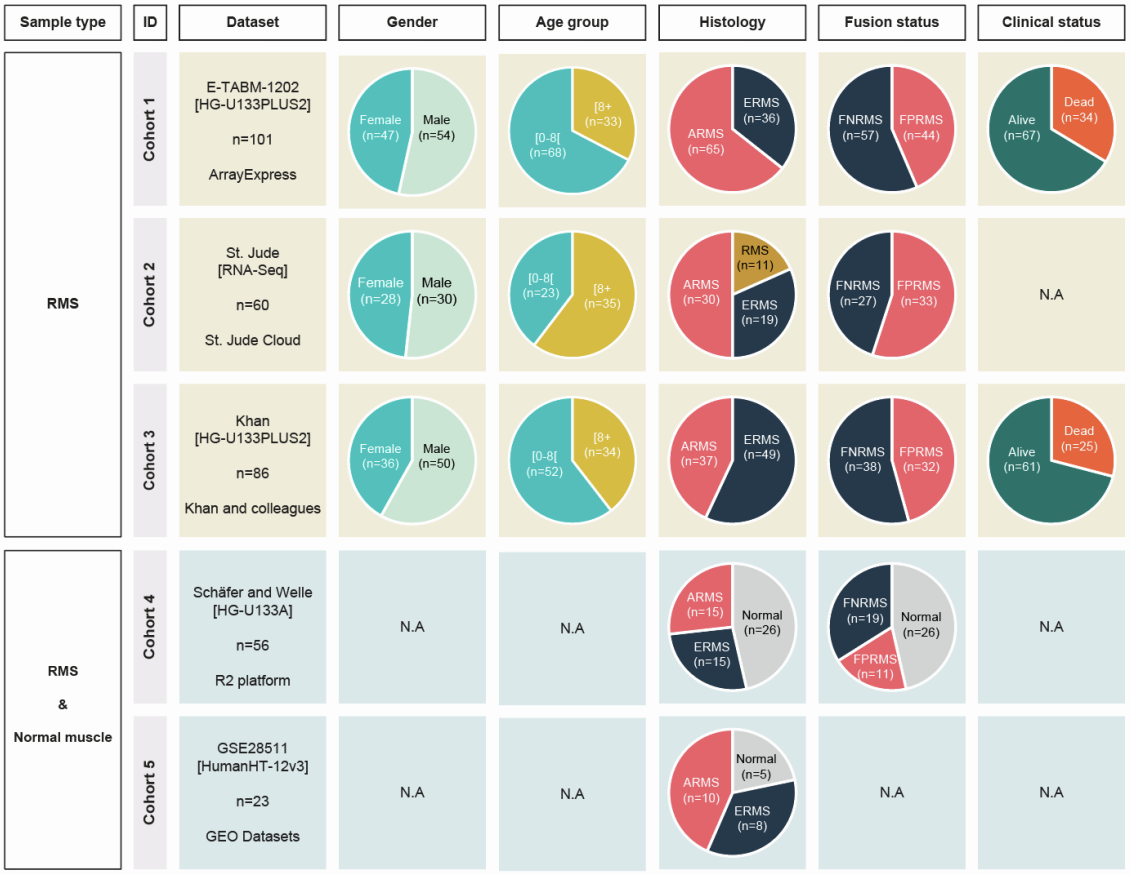

Figure S1. Clinical description of the five cohorts used for transcriptomic analyses. Related to Figure 3. Sample proportions depending on the clinical categories are represented: gender, age group (in years), histology, fusion status, clinical status in the 5 following datasets, i.e. E-TABM-1202 (cohort 1; Missiaglia et al., PMID: 22454413), St. Jude (cohort 2; McLeod et al., PMID: 33408242), Khan (cohort 3; Shern et al., PMID: 24436047), Schafer and Welle (cohort 4; Schafer-Welle-56-MAS5.0-u133a) and GSE28511 (cohort 5; Li et al., PMID: 22330340). ARMS: alveolar rhabdomyosarcoma; ERMS: embryonal rhabdomyosarcoma; FDR: False Discovery Rate; FNRMS: Fusion-Negative Rhabdomyosarcoma; FPRMS: Fusion-Positive Rhabdomyosarcoma; RMS, Rhabdomyosarcoma.

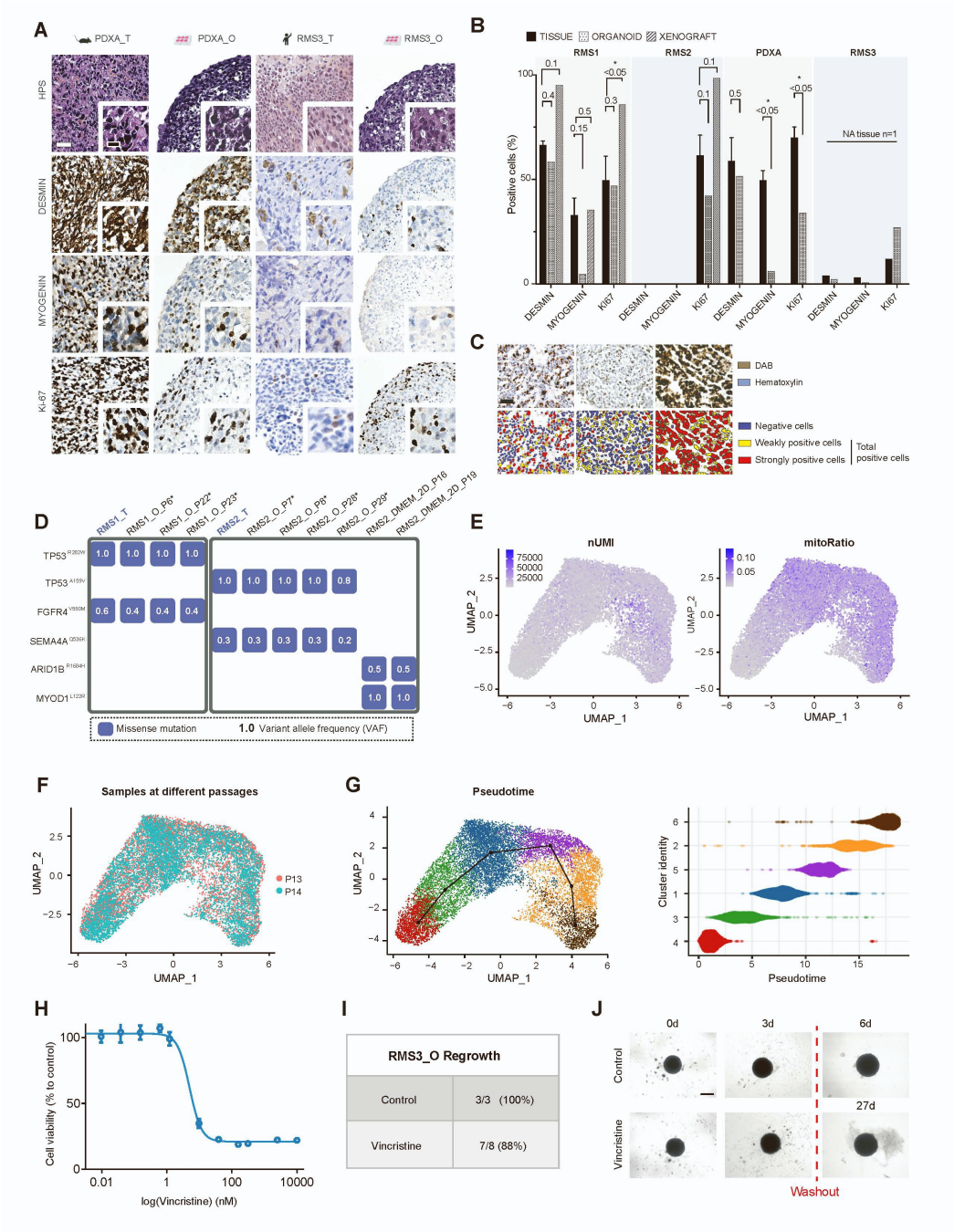

Figure S2. Characterization of FNRMS-derived organoids. Related to Figures 1 and 2. A. Representative HPS and IHC characterization of RMS_O and PDX_O, using clinical markers routinely used for RMS diagnosis. RMS_O were matched blind by anatomopathologists to their tumor-of-origin. PDXA_T, tumor from Patient-derived xenograft A; RMS3_T, tumor from Patient 3. White scale bar: 50 µm, black scale bar: 10µm. **B.** Histogram of the quantification of Desmin, Myogenin and Ki67 positive cells (Percentage of total cells) for RMS1, RMS2, PDXA and RMS3 tissues, organoids, and xenografts (when applicable). Mann–Whitney U tests were applied on at least n=3 areas (for tissues) or n=2 biological replicates (RMS organoids) to assess statistical significance. **C.** Example of automated mask detection used for the generation of the histogram (B). Scale bar = 100 µm. **D.** Preservation of tumor mutational profile in RMS_O. DNA sequencing on genomic DNA (gDNA) of RMS1 and RMS2 tumors (RMS_T) and their corresponding tumoroids, respectively RMS1_O and RMS2_O. RMS_O culture passages (P) are indicated. Models derived in DMEM as 2D cell lines are referred to as RMS_DMEM_2D. **E-G.** UMAP visualization of unified scRNA-seq data of FNRMS-organoid derived from Patient 1 (RMS1_O) samples. **E.** Quality control metrics (nUMI, number of transcripts; and mitoRatio, percentage of mitochondrial transcripts). **F.** Biological replicates (RMS1_O samples at P13 and P14 passages). **G.** Unsupervised trajectory inference analysis using slingshot. Left panel: UMAP visualization. Right panel: cell distribution for each cluster (y-axis) along pseudotime (x-axis). **H-J**. Vincristine dose-response curve and regrowth experiment. H. Vincristine dose-response curve performed on RMS3_O (CellTiter-Glo®). Data were normalized to negative control wells (DMSO only). Means +/- std are represented (n=3). I. RMS3_O regrowth rate within 30 days after treatment washout. J. Representative brightfield images of RMS3_O at t=0 and 3 days, with or without (control) Vincristine treatment. 40 nM; scale bar: 400 µm. Curve (H), rate (I) and images (J) are from one representative experiment out of 3.

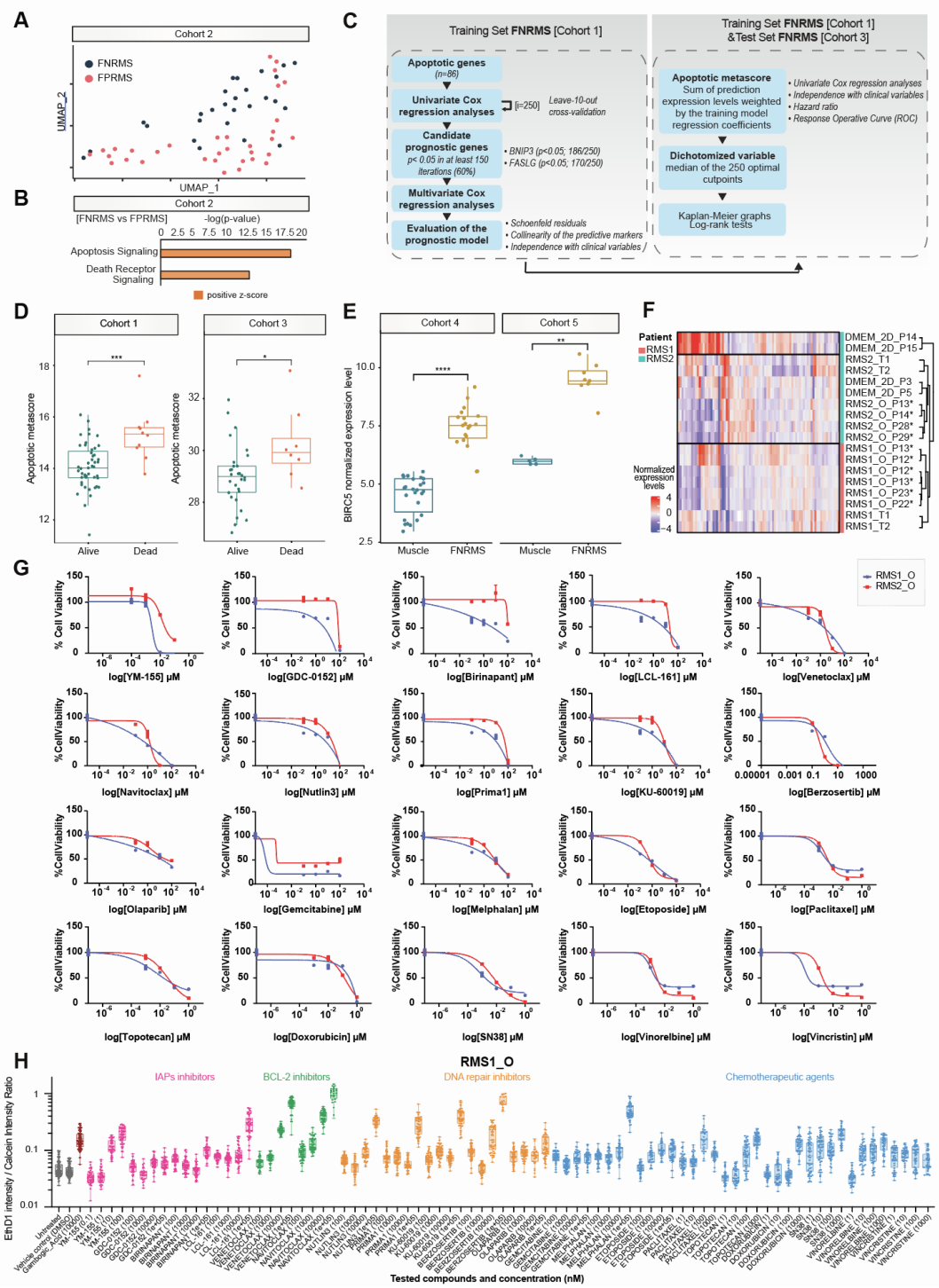

Figure S3. Overexpression of the anti-apoptotic *BIRC5* as a key apoptosis blockage point in FNRMS. Related to Figure 3.
A. UMAP of FNRMS and FPRMS samples (cohort 2) based on the expression of apoptotic effectors (Table S3). **B.** Activation state of apoptotic cascades using Ingenuity Pathway Analysis (IPA) Software in FNRMS versus FPRMS (cohort 2). Significant difference corresponds to z-score > 0 and $p < 0.0001$. **C.** Workflow for construction and evaluation of an apoptotic gene signature and metascore in a training set (cohort 1) and an independent test set (cohort 3). **D.** Apoptotic metascore values between alive and dead patients with FNRMS in the cohorts 1 and 3. Differences between groups were tested using Wilcoxon signed-rank test and associated statistical probability are displayed on top (*: $p \leq 0.05$; ***: $p \leq 0.001$). **E.** Expression levels of *BIRC5* between normal muscles and FNRMS samples (cohorts 4 and 5). Differences between groups were tested using Wilcoxon signed-rank test with associated statistical probability displayed on top (**: $p \leq 0.01$; ****: $p \leq 0.0001$). **F.** Hierarchical cluster analysis based on the centered-normalized expression values of apoptotic genes highlights the high level of similarities between tumoroids (RMS_O) and their corresponding tumor samples (RMS_T). Besides RMS_O, each sample is designed as follows, according to i) the medium in which it was derived, ii) its 2D or 3D structure, and iii) its passage at time of collection: Culture Medium_Dimension_Passage. M3: optimized tumoroid medium; M2: incomplete medium. **G.** Drug response curves of drugs applied on 3D-RMS organoids. Spheres were treated for 72h with indicated compounds (Mean ± std, n=3 technical replicates). **H.** Boxplots depicting the cytotoxicity of indicated agents. Boxplots indicate the level of induced cytotoxicity as measured by the log of dead/live ratio after treatment. Boxes represent the 25%, 50% and 75% quartiles, and whiskers represent the minimum and maximum values. Each circle represents 1 RMS_O, with an average of 46 RMS_O per condition.

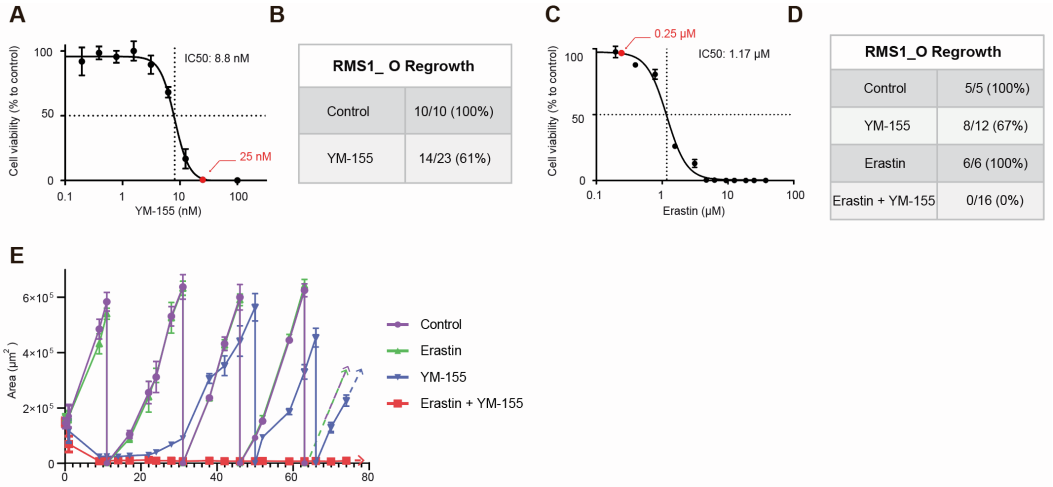

Figure S4: Improving drug combinations' evaluation using FNRMS-derived organoids: proof-of-concept on apoptosis. Related to Figure 4.

A. IC_{50} curve representing RMS1_O sensitivity to YM-155 (CellTiter-Glo®). Data were normalized to negative control wells (DMSO only). Means +/- std are represented (n=3). Red dot indicates the concentration that was used in further experiments. **B.** RMS1_O regrowth rate within 30 days after treatment washout (n=3 experiments). **C.** IC_{50} curve representing RMS1_O sensitivity to Erastin (CellTiter-Glo®). Data were normalized to negative control wells (DMSO only). Means +/- std are represented (n=3).. Red dot indicates the concentration that was used in further experiments. **D**. RMS1_O regrowth rate within 80 days after treatment washout, showing improved efficacy of the combination Erastin/YM-155. The table is from one representative experiment out of 3; Control n=5; Erastin n=6; Ym-155 n=12; Erastin+YM-155 n=16). **E.** Growth curves of RMS1_O after treatment washout in the different conditions tested. Each point corresponds to the mean +/-std of at least 2 RMS1_O areas. Vertical falls of growth curve lines to 0 correspond to the split of the tumoroids (curves are from one experiment representative of n=3 experiments).